





Local production of corticotropin-releasing hormone in prefrontal cortex modulates male-specific novelty exploration

Michael H. Riad^a, Kwanghoon Park^a, Ines Ibañez-Tallon^a , and Nathaniel Heintz^{a,1} 

Contributed by Nathaniel Heintz; received July 4, 2022; accepted October 29, 2022; reviewed by Joseph Dougherty and Gord Fishell

Neuromodulatory substances can be released from distal afferents for communication between brain structures or produced locally to modulate neighboring circuit elements. Corticotropin-releasing hormone (CRH) from long-range neurons in the hypothalamus projecting to the medial prefrontal cortex (mPFC) has been shown to induce anxiety-like behaviors. However, the role of CRH produced in the mPFC has not been investigated. Here we demonstrate that a specific class of mPFC interneurons that express CRH (CrhINs) releases CRH upon high-frequency stimulation to enhance excitability of layer 2/3 pyramidal cells (L2/3 PCs) expressing the CRH receptors. When stimulated at low frequency, CrhINs release GABA resulting in the inhibition of oxytocin receptor-expressing interneurons (OxtrINs) and L2/3 PCs. Conditional deletion of CRH in mPFC CrhINs and chemogenetic activation of CrhINs have opposite effects on novelty exploration in male but not in female mice, and do not affect anxiety-related behaviors in either males or females. Our data reveal that CRH produced by local interneurons in the mPFC is required for sex-specific novelty exploration and suggest that our understanding of complex behaviors may require knowledge of local and remote neuromodulatory action.

corticotropin releasing hormone | medial prefrontal cortex | novelty exploration | sexual dimorphic | circuit modulation

Transcriptional and epigenetic profiling of cell types in mouse (1, 2) and human brains (3, 4) has refined our appreciation of the histological complexity of the cerebral cortex first documented more than a century ago (5). Although it has been demonstrated that the cortex is composed of scores of molecularly distinct cell classes with different electrophysiological properties (6–9), our knowledge of the roles of these cell types in behavior is incomplete. For example, despite the facts that neuropeptides and their receptors are amongst the most diverse and cell-type restricted molecules in the cerebral cortex (10) and the fundamental roles of neuromodulation in all species (11, 12), our knowledge of the cell types expressing these factors and of the functions of neuropeptides in the cerebral cortex are just beginning to emerge.

Most interneurons in the mammalian cerebral cortex express both fast-acting neurotransmitters and specific neuropeptides, hormones, or other neuromodulatory substances (13, 14) to regulate local cortical circuits controlling perception, learning and memory, motor skills, and cognitive functions. For example, the neuropeptide oxytocin (OXT) acts on oxytocin receptor-expressing interneurons (OxtrINs) in the medial prefrontal cortex (mPFC) to modulate local circuit function and regulate sexually dimorphic behaviors. In female mice, OXT activation of OxtrINs during estrus enhances female interactions with male mice (15). OxtrINs are highly enriched with corticotropin-releasing hormone (CRH) binding protein (CRHBP) (16), an endogenous antagonist to CRH. In males, CRHBP released from OxtrINs blocks the effect of CRH on mPFC L2/3 cells, altering anxiety-related behaviors (16). While OXT is produced only in the hypothalamus, CRH is expressed both in the hypothalamus and in small populations of neurons in other brain structures including the cerebral cortex (17–19). In this case, and in many others in which a neuropeptide or neuromodulator can be produced both locally within the cortex and in afferent projections to the cortex, the circuit mechanisms impacted by its release and their consequences for cortical function may depend critically on its source. To address this issue, and to determine whether CRH release from cortical neurons has roles distinct from hypothalamic release of the hormone, we have studied in detail a small subset of cells expressing CRH in the mPFC.

Here we show by Translational Ribosome Affinity Purification (TRAP) profiling, immunolabeling, and viral injections that the majority (~71%) of CRH-expressing interneurons (CrhINs) in the mPFC are vasoactive intestinal peptide/serotonin 5-hydroxytryptamine receptor 3A (VIP/5-HT_{3A}R)-expressing interneurons, with profuse projections that cover the superficial cortical layers. We demonstrate that CrhIN intrinsic electrophysiological properties are consistent with this classification (20), and that they do not differ between males and females.

Significance

CRH is a well-known neuropeptide hormone associated with stress response and anxiety. It is mainly secreted by paraventricular neurons in the hypothalamus. However, CRH is also produced by a sparse population of cortical interneurons that project locally in the medial prefrontal cortex. Using genetic manipulations, we show that CRH released by this interneuron population regulates exploration of novel objects and novel mice in a sex-specific manner.

Author affiliations: ^aLaboratory of Molecular Biology, Howard Hughes Medical Institute, The Rockefeller University, New York, NY 10065

Author contributions: M.H.R., I.I.-T., and N.H. designed research; M.H.R. performed research; M.H.R., K.P., I.I.-T., and N.H. analyzed data; and M.H.R., K.P., I.I.-T., and N.H. wrote the paper.

Reviewers: J.D., Washington University in St. Louis School of Medicine; and G.F., Harvard Medical School.

The authors declare no competing interest.

Copyright © 2022 the Author(s). Published by PNAS. This open access article is distributed under Creative Commons Attribution-NonCommercial-NoDerivatives License 4.0 (CC BY-NC-ND).

¹To whom correspondence may be addressed. Email: heintz@rockefeller.edu.

This article contains supporting information online at <https://www.pnas.org/lookup/suppl/doi:10.1073/pnas.2211454119/-/DCSupplemental>.

Published November 29, 2022.

However, the activation of CrhINs in mouse brain slice preparations from the mPFC reveals frequency-dependent, sexually dimorphic postsynaptic responses of both OxtRINs and L2/3 pyramidal cells expressing the CRH receptor (CRHR1). Studies of mice in which CRH has been excised from CrhINs in the mPFC or in which CrhINs have been chemogenetically activated demonstrate that CRH release in the mPFC modulates male-specific novelty exploration but has no impact on anxiety-related behaviors in either males or females. Taken together, these data provide additional support for the reciprocal and opposing roles of CrhINs and OxtRINs in the modulation of sex-specific behaviors (16) and demonstrate that local release of CRH by CrhINs in the mPFC has functional roles distinct from those mediated by long-range release from the hypothalamus (21).

Results

CrhINs are a Small Subclass of VIP/5-HT_{3A}R Interneurons. To address the role of CRH in cortical microcircuits and identify which cell types express CRH in the mPFC, we employed the knockin CRH-IRES-Cre mouse line (B6(Cg)-*Crh*^{tm1(cre)}^{Zjh}/J, JAX # 012704) generated as a resource of Cre driver lines for genetic targeting of GABAergic neurons in cerebral cortex (Taniguchi et al., 2011). This is a well-established mouse line shown to express Cre recombinase in CRH neurons (22–24). Immunohistochemistry for EYFP expression in CRH-IRES-Cre x Ai3 mice has shown that 90% of fluorescent-labeled neurons are immunoreactive to CRH antibodies (25). We crossed CRH-IRES-Cre mice to a Cre-dependent TRAP reporter line (Rosa26-L10a-eGFP, JAX #024750) to visualize CRH-expressing cells and determine their molecular profile. We observed robust eGFP immunoreactivity in a sparse population of cells in the mPFC (Fig. 1A and *SI Appendix*, Fig. S1A) and very dense labeling of the paraventricular nucleus (PVN) of the hypothalamus (*SI Appendix*, Fig. S1B). To identify mRNAs expressed and translated in this small population of cortical cells, we used TRAP profiling (26). TRAP data collected from the mPFC of these mice (n = 8 for each of 3 replicates) demonstrated enrichment of CRH in addition to known VIP/5-HT_{3A}R interneuron markers including *Gad1*, *Dlx1*, *Vip*, and *Htr3a* mRNAs in immunoprecipitated (IP) samples. Markers of other interneuron classes such as *Pvalb*, *Crhbp*, and *Oxtr* were not upregulated in CrhINs (IP) in comparison with INPUT samples (Fig. 1B and *SI Appendix*, Fig. S3 and *Datasets S1* and *S2*).

IF co-staining for known interneuron markers on mPFC sections of these mice (Fig. 1C) confirmed that CRH-Cre-eGFP/L10a cells are predominantly VIP/5-HT_{3A}R interneurons (70.83% ± 7.352 SEM) (Fig. 1D), although we noted that a very small percentage were positive for somatostatin (SST) (6.71% ± 1.80 SEM). No co-localization with parvalbumin (PVALB) was observed. We next used RNAscope multiplex in situ hybridization (ISH) to localize *Crh*, *Vip*, and *Htr3a* mRNAs. The co-localization of these three markers in mPFC sections from wild-type mice (*SI Appendix*, Fig. S2 A and B) confirmed that mPFC CRH expressing cells are mostly interneurons of the VIP/5-HT_{3A}R subtype, and thus we refer to as CrhINs. Given the relative rarity of mPFC CrhINs in CRH-IRES-Cre mice compared to the numerous VIP labeled cells that do not express *Crh* in the ISH experiments, we next determined the fraction of VIP interneurons that co-express CRH. To quantify and visualize the cell morphologies of CrhINs and VIP interneurons in adult mPFC, CRH-IRES-Cre mice crossed to VIP-Flp mice were injected with AAV2-DIO-mCherry and AAV2-fDIO-eYFP (Fig. 1E) to detect CRH-expressing neurons with red fluorescence and VIP cells with green fluorescence (Fig. 1F). The

quantification of these results revealed that 73% (108/149) of mPFC CRH neurons are VIP interneurons and that CrhINs account for 18% (62/344) of all mPFC VIP interneurons (Fig. 1G).

Anatomical and Electrophysiological Properties of CrhINs.

To evaluate local and long-range CRH neuronal circuits in the mPFC, we injected CRH-IRES-Cre mice with the red fluorescent channelrhodopsin-2 (ChR2-mCherry) expressing virus, AAV2-DIO-ChR2-mCherry in either the PVN (Fig. 1H) or the mPFC (Fig. 1J). Imaging of these mice revealed that CRH neurons of the PVN have long-range axonal projections that reach the mPFC that can be detected with ChR2-mCherry (Fig. 1H). In contrast, CRH neurons in the mPFC, which are much less numerous and sparse than those in the PVN (*SI Appendix*, Fig. S1), show a stellate morphology and arborize extensively but locally in the mPFC particularly in the superficial cortical layers (Fig. 1J). Concurrent injection of two different fluorescent variants of AAV Cre-dependent ChR2 in the mPFC and in the PVN of CRH-IRES-CRE mice demonstrated overlapping long-range and short-range local projections in the mPFC, suggesting substantial release of CRH in the mPFC from both long-range afferent PVN neurons and local CrhINs (*SI Appendix*, Fig. S4 A–C).

To analyze the intrinsic electrophysiological properties of CrhINs, we injected CRH-IRES-Cre mice with AAV2-DIO-ChR2-mCherry in the mPFC and performed fluorescence-guided whole-cell current clamp recordings in CrhINs (Fig. 1I and J). We observed large voltage decreases in response to a –25-pA hyperpolarizing current injections and repetitive burst firing in response to a +25-pA depolarizing current injections in both males (Fig. 1K, *Left*) and females (Fig. 1K, *Right*), and high-frequency AP firing in response to current injections as low as 50 pA (Fig. 1L and *SI Appendix*, Fig. S5A). AP frequency–current (F–I) curves generated by the 25-pA stepwise current injections (Fig. 1L) revealed that CrhINs quickly increase AP firing in response to current injections and plateau at sustained AP frequencies upon high current injection. The measurement of whole-cell intrinsic properties revealed that CrhINs have a high input membrane resistance (Fig. 1M and *SI Appendix*, Table S1). Resting membrane potential (V_m), AP threshold, amplitude, and half-width and membrane time constants were comparable between males and females (*SI Appendix*, Fig. S5 B–F and Table S1). Both male (*SI Appendix*, Fig. S5 G and H) and female CrhINs (*SI Appendix*, Fig. S5I) displayed repetitive AP firing following a single 470-nm LED pulse (5 ms). High membrane resistance, which likely accounts for the large voltage responses and burst AP firing following single-pulse LED stimulation in both males (*SI Appendix*, Fig. S5 G and H) and females (*SI Appendix*, Fig. S5I), is a result of their small somata and has been reported previously as a property of cortical VIP/5-HT_{3A}R expressing interneurons (20). Taken together, these data establish that CrhINs exhibit most of the molecular, anatomical, and electrophysiological properties that characterize VIP/5-HT_{3A}R interneurons and, therefore, can be considered a small subclass of VIP/5-HT_{3A}R interneurons.

CrhINs inhibit OxtRINs. VIP/5-HT_{3A}R interneurons are known to preferentially synapse with and inhibit SST interneurons (27, 28). Since OxtRINs are a subset of SST interneurons that release the endogenous inhibitor of CRH, CRHBP (16) and are present in the mPFC near CrhINs, this suggested to us a possible crosstalk between OxtRINs and CrhINs. To examine this possibility, Crh-Flp mice were crossed to OxtR-Cre mice and injected with Flp- and Cre-dependent viruses in the mPFC (Fig. 2A). Thus, to selectively

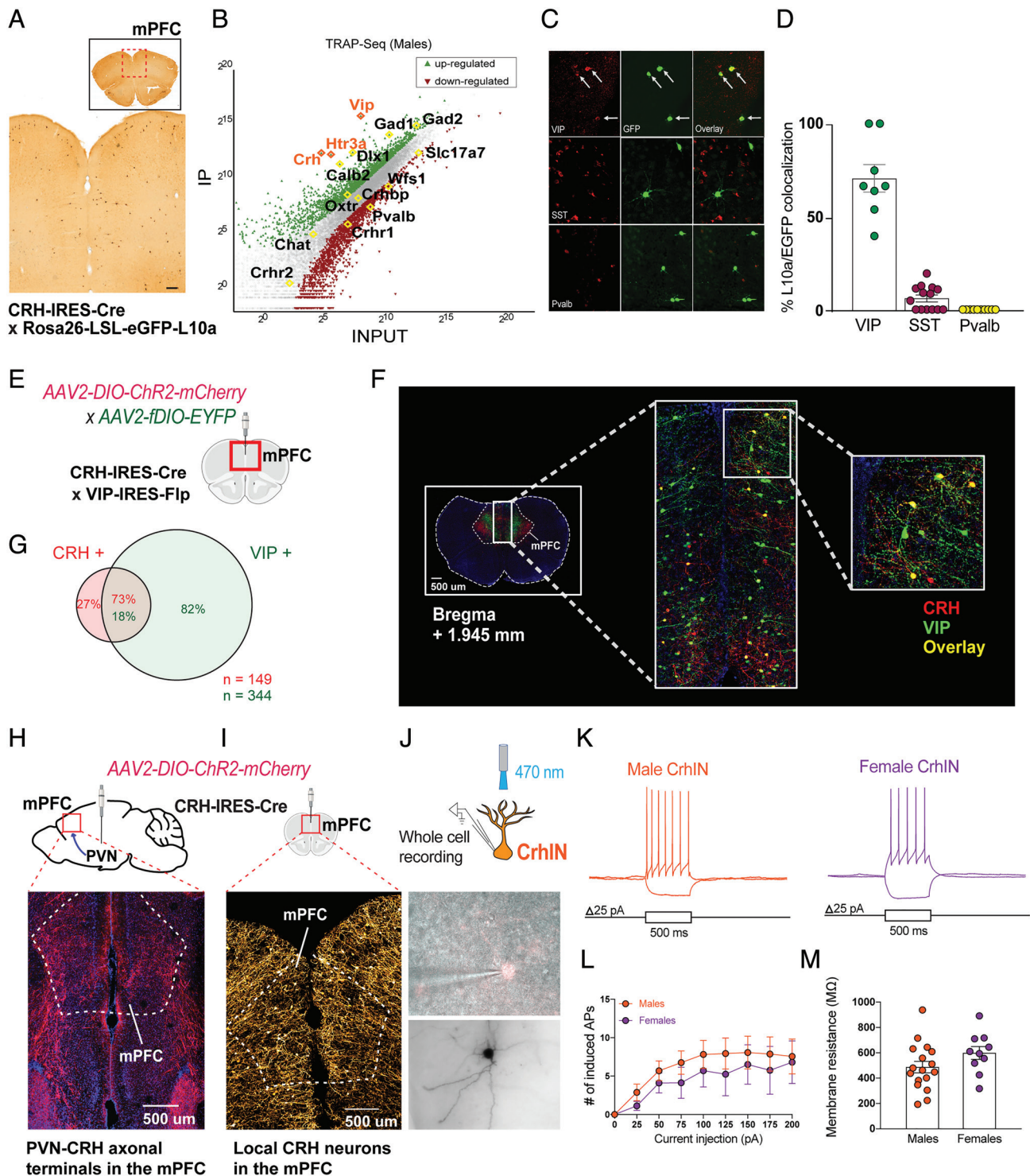


Fig. 1. Molecular and electrophysiological profiles of CrhINs in the mPFC. (A) CRH-IRES-Cre x Rosa26-LSL-eGFP-L10a (= CRH × L10a) mice were used to detect CrhINs by DAB immunostaining against eGFP in the mPFC. (B) TRAP-Seq molecular profiling of mPFC samples of CRH × L10a mice revealed an abundance of transcripts associated with VIP/5-HT_{3A}R interneurons in CrhINs. (C) Immunofluorescence (IF) for interneuron markers and eGFP in CRH × L10a mice. (D) Quantification of IF results revealed that 70.83% ± 7.352 and 6.71% ± 1.80 of L10a/EGFP cells colocalize with VIP and SST, respectively, and no evidence of Pvalb colocalization. (E and F) CRH-IRES-Cre mice crossed with VIP-IRES-Flp mice injected with the indicated AAV2 viruses were used to visualize CRH and VIP interneurons in the mPFC. (G) Quantification of interneurons in double-injected CRH-IRES-Cre × VIP-IRES-Flp mice indicated that 73% of mPFC CRH neurons expressed VIP and that CRH neurons represented 18% of all mPFC VIP neurons. (H and I) AAV2-DIO-ChR2-mCherry was injected into the PVN or the mPFC of CRH-IRES-Cre mice. Distal projections of PVN-CRH neurons to the mPFC (H) and local CrhINs in the mPFC (I) were observed. (J) Schematic and photomicrographs showing the whole-cell configuration used for recordings of CrhINs (visualized with red fluorescence) with LED optogenetic stimulation. DAB immunostaining following dialysis of neurobiotin revealed the stellate morphology of mPFC CrhINs. (K) Male and female CrhINs responded with a large voltage decrease in response to a -25-pA hyperpolarizing current injection and repetitive burst firing in response to a +25-pA depolarizing current injection. (L) The number of fired action potentials (APs) at increasing injected currents (frequency-current F-I) curves showed that CrhINs had low rheobase current and fired multiple action potentials at low current injections in male (n = 17) and female (n = 10) CrhINs. (M) Male and female CrhINs displayed high membrane resistance which is a characteristic of VIP interneurons. Data are represented as mean ± SEM.

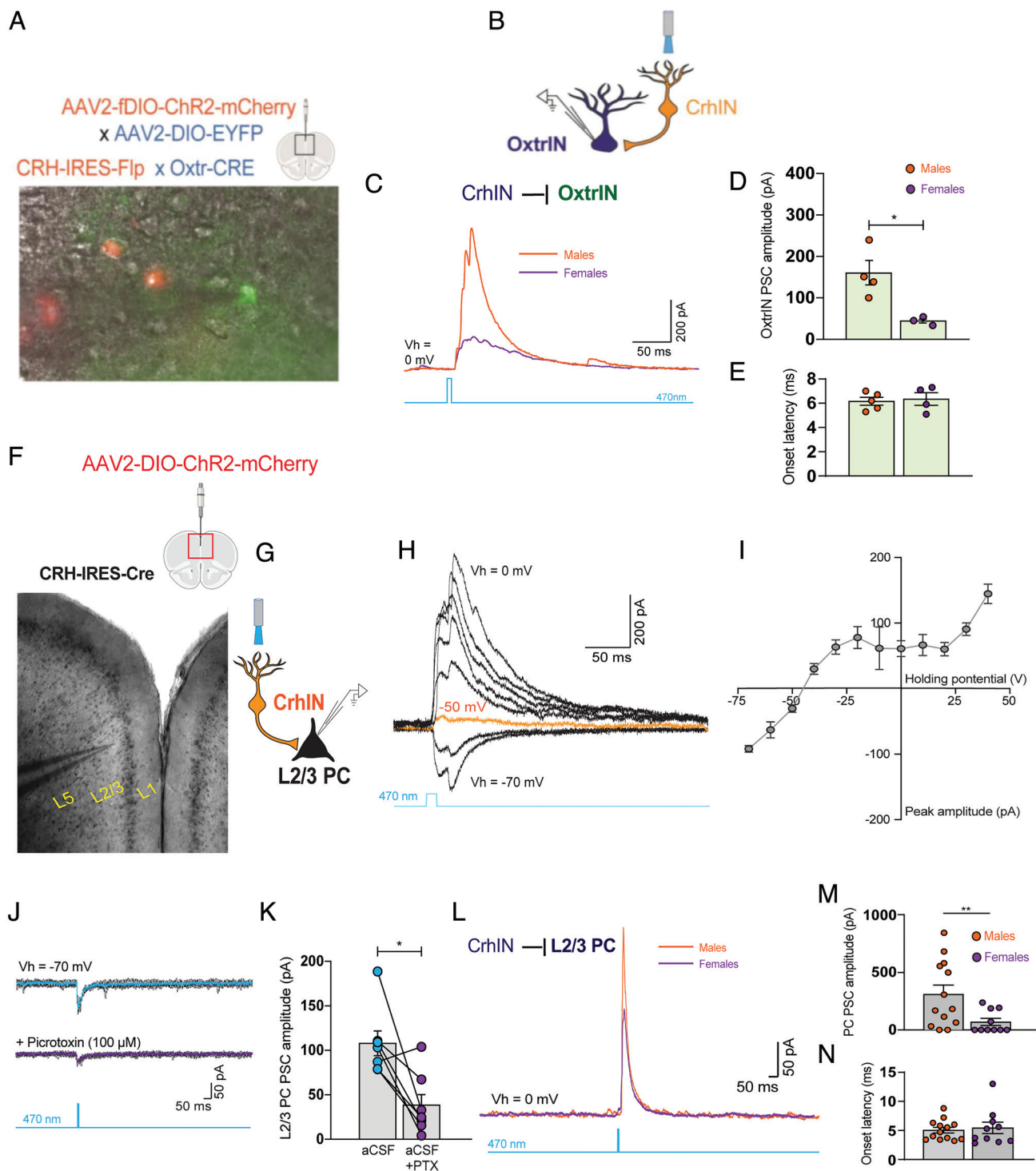


Fig. 2. Optogenetic stimulation of CrhINs elicits stronger currents in male OxtRINs and PCs in the mPFC. (A) CrhINs (red) and OxtRINs (green) in the mPFC of CRH-Flp mice crossed with OxtR-CRE mice injected with the indicated Flp(AAV2-fDIO-ChR2-mCherry)- and Cre(AAV2-DIO-EYFP)-dependent AAV viruses. (B) Schematic and photomicrographs showing the voltage clamp whole-cell configuration used for recordings of OxtRINs (green) upon optogenetic stimulation of CrhINs expressing ChR2 (red). (C) Single-pulse optogenetic stimulation of CrhINs (blue line, 5 ms) elicited PSCs (orange and purple traces) in male and female OxtRINs that displayed several sequential peaks (multiphasic). (D and E) Quantification of PSCs amplitudes (D) and onset latency (E) in male and female OxtRINs elicited by optogenetic stimulation of CrhINs. PSCs amplitudes were significantly larger in males ($P < 0.05$). The short onset latencies, which were comparable between males and females, suggest that the CrhINs-OxtRINs pathway was monosynaptic. (F and G) Photomicrograph and schematic showing the voltage clamp whole-cell configuration used for recordings of L2/3 PCs (visualized with differential interference contrast between L5 and L1 PCs) in mPFC brain slices of CRH-IRES-Cre mice injected with AAV2-DIO-ChR2-mCherry upon optogenetic stimulation of CrhINs expressing ChR2 (in red). (H) Voltage clamp recordings of L2/3 PCs at increasing V_h (from -70 mV to 40 mV, $\Delta 10$ mV) revealed that the L2/3 PSCs elicited by optogenetic activation of CrhINs reversed direction near -50 mV. (I) Quantification of L2/3 PCs PSCs evoked by optogenetic activation of CrhINs showed that the reversal potential was near -50 mV. (J) Bath application of the GABA_A receptor antagonist, picrotoxin (PTX, $100 \mu\text{M}$) markedly inhibited the L2/3 PCs PSCs elicited by optogenetic stimulation of CrhINs ($P < 0.05$). (K) Quantification of L2/3 PSCs elicited by optogenetic stimulation of CrhINs before and after bath application of $100 \mu\text{M}$ PTX ($n = 7$). (L) Optogenetic stimulation of CrhINs (blue line) elicited single peak PSCs in male and female L2/3 PCs. PSCs recorded at $V_h = 0$ mV were larger in male mice. (M and N) Quantification of L2/3 PSCs amplitudes (M) and onset latencies (N) revealed that monosynaptic PSCs were significantly larger in males than those of females ($P < 0.01$). * $P < 0.05$, ** $P < 0.01$.

stimulate CrhINs and record OxtrINs, we expressed ChR2 in CrhINs and labeled OxtrINs with EYFP. CrhINs somata were concentrated near L2/3 and L5, whereas OxtrIN somata were more numerous and distributed across all cortical layers (*SI Appendix, Fig. S6A*). As a first step in characterizing the modulation of local mPFC circuits by CrhINs, we optogenetically stimulated CrhINs expressing ChR2-mCherry, while recording OxtrINs expressing EYFP (Fig. 2*B*). To evaluate the synaptic connectivity between CrhINs and OxtrINs, we performed whole-cell voltage clamp recordings of OxtrINs held at $V_h = 0$ mV to measure postsynaptic currents (PSCs), which are GABA-mediated inhibitory currents as shown previously (27, 28). We observed optogenetic responses in 85% of the recorded male and female OxtrINs, indicating high connectivity between OxtrINs and CrhINs.

Optogenetic activation of CrhINs elicited multiphasic PSC waveforms in OxtrINs (Fig. 2*C*). Similar multiphasic responses exhibiting inflections of rising and decaying phases have been reported when activating CRH neurons in other areas of the brain (29). These complex responses are likely a result of the high excitability of this interneuron class shown by the repetitive burst firing of CrhINs in response to single LED pulses (*SI Appendix, Fig. S5 G–J*). Optogenetic activation of CrhINs elicited large PSCs in male OxtrINs (Fig. 2*C* and *D*), but PSC responses in female OxtrINs were significantly reduced (Fig. 2*C* and *D*).

It has been shown that onset latency for monosynaptic transmission elicited by optogenetic stimulation ranges between 3.6 and 17.3 ms, while onset latency for polysynaptic transmission varies between 18.0 and 25.6 ms (30–36). To determine whether CrhIN and OxtrIN are monosynaptically connected, we measured onset latencies for PSCs in OxtrINs following stimulation of CrhINs. There was no difference in onset latencies between males and females (onset latency: males = 6.16 ± 0.32 ; females = 6.35 ± 0.52 , $P > 0.7$, Fig. 2*E*). The short onset latencies measured for CrhIN elicited PSC responses in OxtrINs indicate that there is likely a monosynaptic circuit from CrhINs to OxtrINs in the mPFC. These data also demonstrate that activation of CrhINs produces inhibitory PSCs in OxtrINs which are significantly larger in males suggesting that the biological role of CrhINs may be enhanced in male mice.

PSCs in layer 2/3 Pyramidal Cells Elicited by Single-Pulse Optogenetic Stimulation of CrhINs are GABAergic. To determine how CrhINs modulate mPFC L2/3 pyramidal cells (PCs), we used CRH-IRES-Cre mice injected with AAV2-DIO-ChR2-mCherry (Fig. 2*F*). We identified layer 2/3 pyramidal cells (L2/3 PCs) based on their stereotyped somatic morphology and clear laminar organization in mPFC brain slices with DIC-based optics (Fig. 2*F*).

To study the current–voltage (I – V) characteristic curve and measure the reversal potential of PSCs in CrhIN to L2/3 PC synapses, we clamped L2/3 PCs at V_h ranging from -70 mV to $+40$ mV in 10 mV increments and delivered single LED pulses (Fig. 2*G* and *H*). The serial stimulation protocol revealed that the evoked PSC reversal potential was near -50 mV (Fig. 2*H* and *I*, trace in orange), close to the reversal potential for GABAergic PSCs measured previously in cortical L2/3 PCs (37). To confirm the relative contribution of GABA currents in CrhIN-induced PSCs in L2/3 PCs, we delivered single LED pulses before and after bath application of the GABA_A receptor antagonist, picrotoxin (PTX) (Fig. 2*J* and *K*). This revealed that CrhIN-induced PSCs in L2/3 PCs were sensitive to PTX, indicating that the currents induced in L2/3 PC synapses by single LED pulses were GABA-mediated.

To investigate whether CrhIN-elicited PSCs in L2/3 PC are different in male and female mice, we performed voltage clamp recordings in L2/3 PCs holding the V_h at 0 mV. Measurements of PSC amplitudes demonstrated that the PSC amplitudes in L2/3 PCs

elicited by single-pulse optogenetic activation of CrhIN were more pronounced in males than in females (Fig. 2*L* and *M*). Onset latencies measured in males and females were comparable (Fig. 2*N*). The short onset latencies (onset latency: males = 5.04 ± 0.48 ; females = 5.43 ± 0.99 , $p > 0.7$) suggest that the circuit from CrhINs to PCs in the mPFC is also monosynaptic. We observed CrhIN-induced PSCs in 62% (13/21) of the L2/3 PCs recorded in male mice and in 66% (14/21) of the L2/3 PCs recorded in female mice. This is consistent with the expression of CRHR1 in the majority but not in all of layer 2/3 PCs (<http://mouse.brain-map.org/gene/show/12704>). To sum up, these results demonstrate that single-pulse stimulation of mPFC CrhINs is sufficient to induce GABAergic PSCs in L2/3 PCs of significantly larger amplitude in males than in females.

CrhINs Release CRH upon High-Frequency Stimulation. While single-pulse optogenetic stimulation is sufficient to induce release of GABA from CrhINs to L2/3 PCs (Fig. 2*F–M*), studies of dense core fusion and neuropeptide release have suggested that, in contrast to release of neurotransmitters (11, 38), efficient release of neuropeptides requires high-frequency stimulation (39, 40). Therefore, we next investigated whether high-frequency optogenetic stimulation could elicit CRH release from CrhINs to L2/3 PCs in vitro.

To ensure that CrhINs expressing ChR2 in mPFC could fire at sustained high rates in response to high-frequency LED stimulation, we first stimulated at 1 Hz and 20 Hz and recorded CrhINs expressing ChR2 (Fig. 3*A*) in whole-cell configuration. These experiments revealed robust firing in response to both 1 Hz (Fig. 3*B*, orange trace) and 20 Hz (Fig. 3*C*, orange trace) optogenetic stimulation. This is consistent with electrophysiological studies of VIP/5-HT_{3A}R interneurons showing that these neurons can fire at high frequency (>50 Hz) when stimulated with a 5-HT_{3A}R agonist (20). We next performed voltage clamp recordings in L2/3 PCs held at $V_h = -70$ mV to measure PSCs elicited by optogenetic stimulation of CrhINs. Stimulation at 1 Hz (Fig. 3*B*, blue trace) revealed time-locked PSCs that were variable in amplitude (Fig. 3*B*, black trace). Following 60 s of recovery, we delivered 20 Hz stimulation for 20 s (Fig. 3*C*, blue trace), which elicited a two-component PSC response in L2/3 PCs (Fig. 3*C*, black trace) consisting of a sharp initial inward current followed by an intense long-lasting train of PSCs (Fig. 3*C*, black trace) that likely reflects the response to the endogenous release of CRH from local ChR2 expressing CrhINs. Previous investigations have shown that exogenously applied CRH increases action potential firing through the inhibition of Ca²⁺-dependent K⁺ channels that contribute to the generation of the after-hyperpolarization currents (41), and that modulation of somatic voltage-gated ionic currents is important for the generation of APs (42). Approximately 62% (13/21) of the male L2/3 PCs responded to 20 Hz stimulation, while 38% (8/21) of the male L2/3 PCs did not respond to high-frequency stimulation (*SI Appendix, Fig. S7*). This is consistent with the fact that CRHR1 is expressed in a subset of L2/3 PCs, which we reported previously (16).

To confirm that the observed PSCs upon high-frequency stimulation depend on CRH release, we performed the same experiment with either a selective CRHR1 antagonist (Fig. 3*D–F*) or an inhibitor of G protein-coupled receptor (GPCR) signaling (Fig. 3*G–I*). Pretreatment of cortical slices with the selective CRHR1 antagonist, NBI 27914 HCl (5 μ M) (Fig. 3*D*) did not affect CrhIN-induced L2/3 PSCs at 1 Hz stimulation (Fig. 3*E*, red trace). In contrast, 20 Hz stimulation in the presence of the CRHR1 antagonist resulted in a sharp initial inward current but no longer elicited the intense train of PSCs evident in its absence (Fig. 3*F*, red trace). Since CRHR1 is a class B/secretin-like GPCR that upon

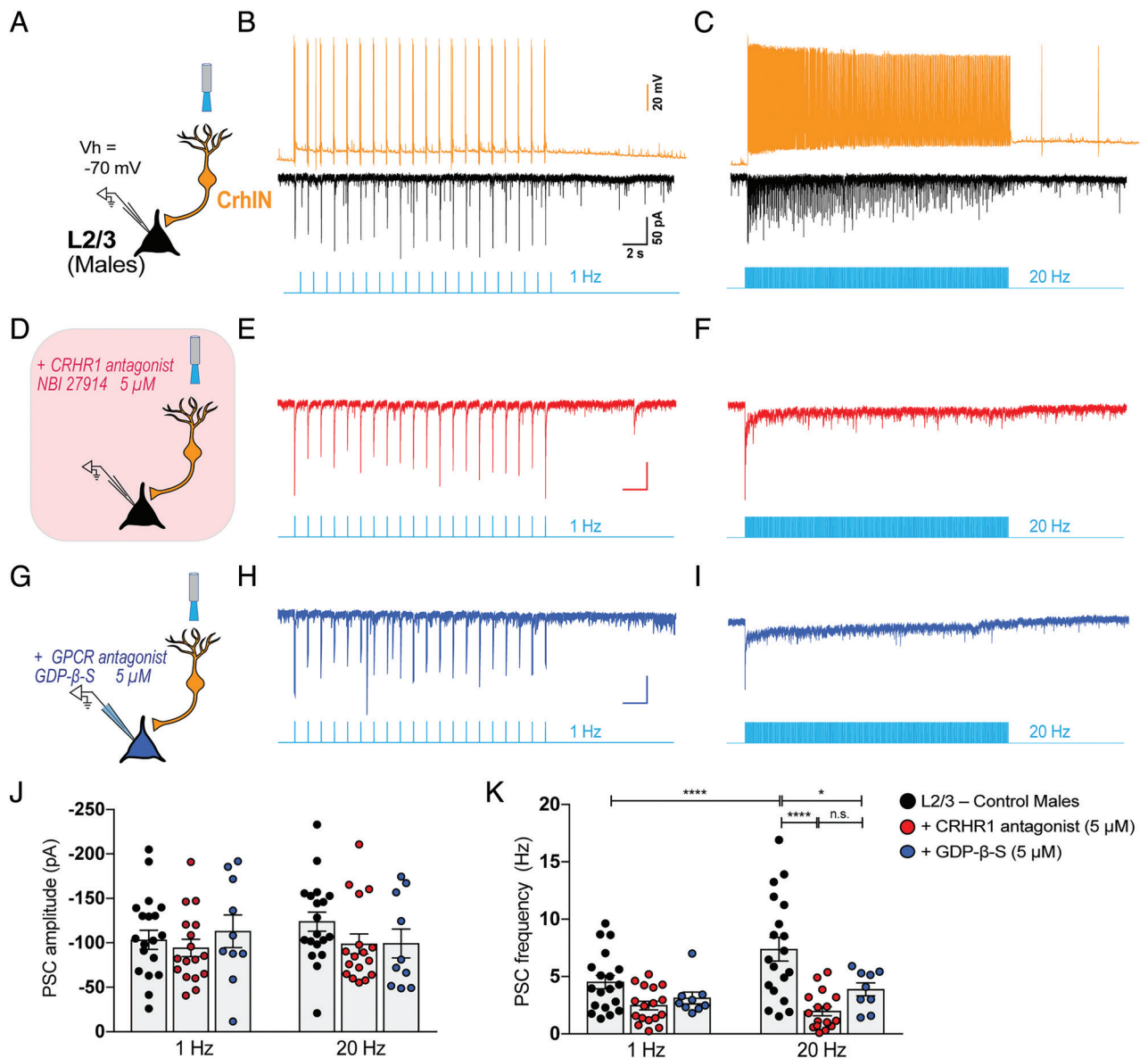


Fig. 3. High-frequency optogenetic stimulation of CrhINs evokes CRH release selectively in male mice. (A) Schematic showing the voltage clamp whole-cell configuration used for recordings of CrhINs (in orange) and L2/3 PCs (in black) in mPFC brain slices of CRH-IRES-Cre mice injected with AAV2-DIO-ChR2-mCherry upon optogenetic stimulation of CrhINs expressing ChR2 (in orange). (B) During 1 Hz LED stimulation delivered for 20 s (blue trace), CrhINs maintained stereotyped AP firing (orange trace) and L2/3 PC held at $V_h = -70$ mV displayed time-locked single PSCs (black trace). (C) During high-frequency 20 Hz LED stimulation (blue continuous trace), CrhINs were able to maintain persistent fast firing (orange trace) and L2/3 PCs responded with an initial inward postsynaptic current followed by a high-frequency train of PSCs (black trace). (D) Voltage clamp recordings from mPFC L2/3 pyramidal cells after 1 h recovery in aCSF containing the CRHR1 antagonist, NBI 27914 (5 μ M). (E) Low-frequency, 1 Hz optogenetic stimulation in the presence of the CRHR1 inhibitor did not affect time-locked PSC responses in L2/3 PCs (red trace). (F) High-frequency, 20 Hz optogenetic stimulation of CrhINs in the presence of the CRHR1 antagonist did not affect the initial inward current but eliminated the subsequent high-frequency train of PSC in L2/3 cells (red trace). (G) Voltage clamp recordings from mPFC L2/3 pyramidal cells using 5 μ M GDP- β -S, antagonist of GPCR transduction in the intracellular solution. (H) Low-frequency, 1 Hz optogenetic stimulation in the presence of the GPCR inhibitor did not affect time-locked PSC response in L2/3 PCs (dark blue trace). (I) Intracellular GPCR blockade with GDP- β -S mimicked the effects of CRHR1 antagonist pre-treatment. At high-frequency stimulation, the initial inward PSCs current persisted but the subsequent high-frequency train of PSC in L2/3 cells (dark blue trace) was absent. (J) Quantification of L2/3 PSCs amplitudes did not reveal significant differences across recording conditions. (K) The frequency of PSCs in L2/3 cells significantly increased between 1 Hz and 20 Hz LED stimulation of CrhINs ($P < 0.0001$). At 1 Hz LED stimulation, the frequency was not affected by CRHR1 antagonist pre-treatment or acute GPCR blockade. At 20 Hz LED stimulation, the CRHR1 antagonist pre-treatment ($P < 0.0001$) and acute GPCR blockade ($P < 0.05$) significantly reduced L2/3 PSCs frequency. * $P < 0.05$, **** $P < 0.0001$.

ligand activation signals mainly by Gs coupling (43), we next tested the effect of GDP- β -S (5 μ M), an inhibitor of GPCR transduction. GDP- β -S was added to the intracellular solution filling the recording pipette in whole-cell configuration to block GPCR signaling only in the recorded L2/3 PCs (Fig. 3G), thus preventing global disruption of GPCR signaling in the slice and potential network effects. Following dialysis of the pipette solution and intracellular milieu, we repeated 1 Hz and 20 Hz stimulation protocols. No major effect of GDP- β -S on PSC responses to 1 Hz stimulation

was evident (Fig. 3H, dark blue trace). However, 20 Hz optogenetic stimulation no longer induced the train of high-frequency PSCs following GDP- β -S dialysis (Fig. 3I, dark blue trace). Quantification of these results revealed that the amplitude of the PSCs in L2/3 pyramidal neurons did not vary significantly across 1 Hz and 20 Hz optogenetic stimulation of CrhINs (Fig. 3J), while the frequency of PSCs in 62% of L2/3 pyramidal cells strongly increased at 20 Hz optogenetic stimulation of CrhINs (Fig. 3K and SI Appendix, Fig. S7). We noted statistically significant

differences between L2/3 PSC frequency, not amplitude, across baseline, CRHR1 antagonist, and GDP β -S conditions, ($F(5, 84) = 9.45, P < 0.0001$) ($n = 2-6$ mice per group), between 1 Hz and 20 Hz ($P < 0.05$), 20 Hz baseline vs. 20 Hz CRHR1 antagonist ($P < 0.0001$), and 20 Hz baseline and 20 Hz GDP β -S ($P < 0.05$). We observed no difference between 20 Hz CRHR1 antagonist treatment and 20 Hz GDP β -S treatment ($P = 0.7078$). These data establish that, in males, release of CRH from CrhINs and its effects on postsynaptic L2/3 PCs require high-frequency stimulation.

We next performed the same voltage clamp ($V_h = -70$ mV) recordings in female L2/3 PCs after low- and high-frequency stimulation of CrhINs. Baseline traces show a slightly but not significantly higher frequency of events in females (*SI Appendix, Fig. S8 A and B*). Both 1 Hz (*SI Appendix, Fig. S8 C and D*) and 20 Hz optogenetic stimulation protocols resulted in significantly reduced PSC frequency in female mice (*SI Appendix, Fig. S8 E and F*). Consistent with the sexual dimorphisms observed thus far, we observed time-locked responses at 1 Hz but very reduced, and a complete absence of the long-lasting train of PSCs observed in males at 20 Hz stimulation (Fig. 3 and *SI Appendix, Fig. S8*). Quantification of the PSCs showed that the frequency but not the amplitude was significantly different in females compared to males (*SI Appendix, Fig. S8 G and H*).

CRH Release from Cortical CrhINs Modulates Male-Specific Novelty Exploration. Next, we investigated whether the sex-specific modulation of CrhINs would affect behaviors differently in males and females. We focused on anxiety-like behaviors and sociability as we previously reported that these behaviors are modulated by interneurons in the mPFC (15, 16). We used two genetic approaches to manipulate CrhINs in the mPFC. We first analyzed the behavioral impact of the loss of *Crh* specifically in CrhINs of the mPFC in males and females. Previous studies have demonstrated that specific deletion of *Crh* in the hypothalamus alters several approach/avoidance behaviors, indicating reduced anxiety (21). A more extensive deletion of *Crh* from all GABAergic neurons in the cortex, hippocampus, central nucleus of the amygdala, and bed nucleus of the striatum alters stress resilience and baseline social interactions (44). Since both studies employed intersectional targeting with transgenic mice that might express Cre-recombinase in early development, and since neither study reported sex-specific behavioral alterations suggested by the modulatory function of CrhIN–OxtrIN signaling in mPFC circuitry, we employed viral intersectional techniques to focus our studies on adult functions of CrhINs in the mPFC. To rule out the possibility that male and female responses might be due to sex-specific differences in CrhIN numbers in the mPFC, we quantified the number of CRH-IRES-Cre cells in the mPFC in males (*SI Appendix, Fig. S1C*) and females (*SI Appendix, Fig. S1D*) and found no differences in the number of immunoreactive cells between males and females (*SI Appendix, Fig. S1E*).

To examine the effects of cortical *Crh* deletion in adults, male and female Crh:FLOX mice (Zhang et al. 2017) were stereotactically injected with either AAV-CMV-Cre/eGFP to delete the *Crh* gene from CrhINs, or control AAV-CMV-eGFP virus into the mPFC (Fig. 4A). Injected mice were analyzed by ISH to assess the efficiency of *Crh* deletion in the mPFC relative to the motor cortex and piriform cortex (Fig. 4B) in brain sections prepared from the same animal. These data demonstrated that the majority of *Crh* expression restricted to the mPFC was lost in mice injected with AAV-CMV-Cre/eGFP relative to mice injected with the AAV-CMV-eGFP control virus.

To assess the behavioral effects of cortical *Crh* deletion in the mPFC of adult mice, we performed a series of tests to measure

anxiety-related behaviors and sociability. No alterations in a battery of approach/avoidance tests, including elevated plus maze (*SI Appendix, Fig. S9A*), open-field test (*SI Appendix, Fig. S9B*), and light/dark box (*SI Appendix, Fig. S9C*), were observed in either male or female CRH-FLOX mice injected in the mPFC with AAV-CMV-Cre/eGFP compared to control virus injected mice. These results indicate that, in contrast to the loss of hypothalamic CRH production (21), loss of local, cortical *Crh* is not anxiogenic. To assess sociability, we used a well-established, three-chamber sociability test that allows mice to freely interact with a lego or with a conspecific mouse of the opposite sex (Fig. 4C). Two-way ANOVA revealed that a nearly significant interaction between sex and *Crh* deletion on the duration investigating either a lego ($F(1, 36) = 4.088, P = 0.051$) or a novel mouse ($F(1, 36) = 3.074, P = 0.088$). Interestingly, subsequent post hoc analyses found that deletion of *Crh* from the mPFC of males induced a significant increase in the duration investigating both a lego and a novel female ($P < 0.05$) (Fig. 4D and *SI Appendix, Fig. S10A*), while cortical deletion of *Crh* in females had no effect on investigating either a lego or a novel male (Fig. 4D). These analyses also showed that females with conditional deletion of Crh in CrhINs show no preference for a novel mouse compared to males with conditional deletion of Crh in CrhINs (Fig. 4D). To check whether cortically produced *Crh* in males modulates sociability, we calculated the social preference index by dividing the time difference between the interaction with a lego and a conspecific mouse by the total investigation time. In both males and females, *Crh* deletion did not affect social preference index, suggesting that *Crh* deletion in male mice increases novelty exploration rather than sociability (*SI Appendix, Fig. S11A*).

To test this hypothesis, we performed a novel object recognition test. For this test, mice were allowed to freely investigate two identical objects (Fig. 4E, *Left*). After 60 min, one of the objects was replaced with a novel object, and the same mice were allowed to freely explore the novel and familiar objects (Fig. 4E, *Right*). Two-way ANOVA statistical analyses indicated that there was no significant interaction between sex and *Crh* deletion on duration investigating for both a familiar ($F(1, 36) = 1.447, P > 0.23$) and novel object ($F(1, 33) = 0.4820, P > 0.49$). However, post hoc analyses revealed that males with conditional deletion of Crh in CrhINs display a significant preference to explore a novel object compared to control males ($P < 0.05$) (Fig. 4F and *SI Appendix, Fig. S10B*). They also showed that females with conditional deletion of Crh in CrhINs show a significant preference for familiar objects compared to males with conditional deletion of Crh in CrhINs (Fig. 4F). These findings demonstrate that deletion of *Crh* in the mPFC does not affect anxiety-like behaviors but modulates novelty exploration selectively in males.

To further investigate the sex-specific effects of mPFC *Crh* on novelty exploration, we reasoned that chemogenetic activation of CrhINs in the mPFC should increase CRH release from CrhINs and have the opposite behavioral effects of *Crh* deletion. To test this hypothesis, we performed i.p. injections of the selective hM3Dq ligand, Clozapine N-oxide (CNO) (2 mg/kg) in CRH-IRES-Cre mice stereotaxic injected with AAV2-DIO-hM3Dq-mCherry in the mPFC (Fig. 4G and H). CNO injection significantly increased c-fos expression in CrhINs in both males and females ($P < 0.0001$ for both males and females, Fig. 4I). Importantly again, activation of mPFC *Crh:hM3Dq* via CNO did not alter anxiety-like behaviors in elevated plus maze, open field test, or light/dark box in either males or females (*SI Appendix, Fig. S9 D–F*), consistent with the lack of effect observed in approach/avoidance tests in response to mPFC deletion of *Crh* (*SI Appendix, Fig. S9 A–C*). We performed the three-chamber sociability test and three-way ANOVA analyses

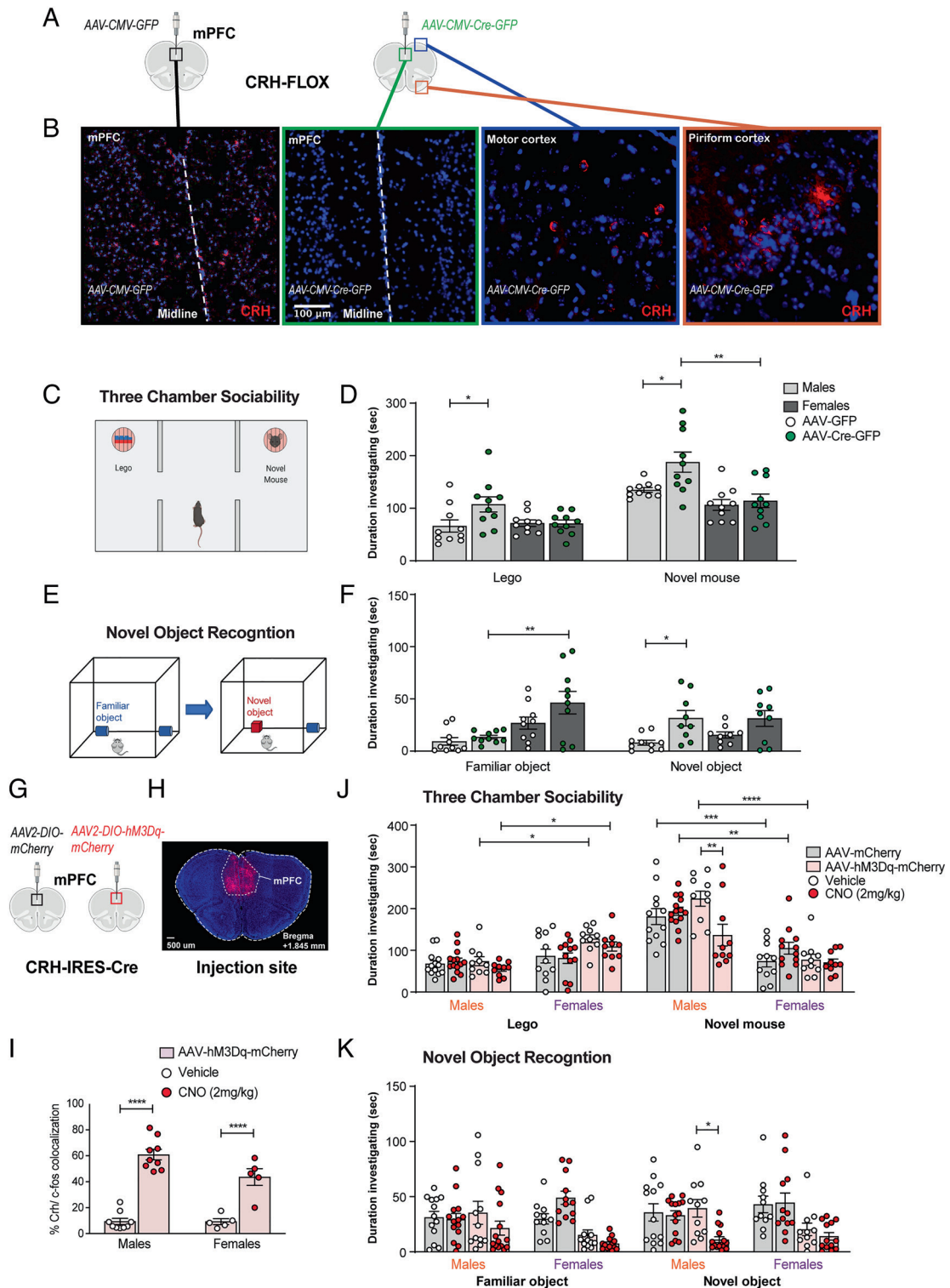


Fig. 4. mPFC conditional knockout of *Crh* and chemogenetic activation of mPFC CrhINs have opposite effects in male novelty exploration. (A and B) CRH-FLOX mice injected in the mPFC with the control virus AAV-CMV-GFP showed *Crh* mRNA ISH signal in scattered cells. CRH-FLOX mice injected in the mPFC with AAV-CMV-Cre-GFP showed selective knockdown of *Crh* mRNA ISH signal in the mPFC but not in non-injected adjacent cortical areas, such as motor and piriform cortex. (C) Experimental overview of the three-chamber sociability behavioral test. (D) mPFC knockdown of *Crh* in male CRH-FLOX mice increased investigation duration of both lego and novel female mice compared to CRH-FLOX male mice injected with control virus ($P < 0.05$ for both). Female CRH-FLOX showed no differences in investigation duration of lego and novel male mice when injected with Cre-expressing virus. Male mice with mPFC knockdown of *Crh* showed significantly more investigation duration with novel mouse compared to female mice with mPFC knockdown of *Crh*. (E) Experimental overview of the novel object recognition test. (F) mPFC knockdown of *Crh* in male ($P < 0.05$) but not in female CRH-FLOX mice increased novel object interaction. Female mice with *Crh* deletion show significant preference for a familiar object compared to male mice with *Crh* deletion. (G) CRH-IRES-Cre was injected in the mPFC with AAV2-DIO-hM3Dq-mCherry (Crh:hM3Dq mice) for chemogenetic activation of CrhINs. (H) hM3Dq-mCherry expression was detected in the mPFC of CRH-IRES-Cre mice. (I) Quantification of c-fos/hM3Dq-mCherry colocalization in Crh:hM3Dq mice after CNO injection compared to vehicle in males and females ($P < 0.0001$). (J) Chemogenetic activation of mPFC CrhINs in male Crh:hM3Dq mice decreased social interaction time with novel female mice ($P < 0.01$). CNO treatment of female Crh:hM3Dq mice did not noticeably affect social interaction time with novel male mice. (K) In male Crh-hM3Dq mice treated with CNO, novel object interaction time was reduced with no effect on familiar object interaction ($P < 0.05$). No effect of activation of mPFC CrhINs in female novelty object preference was observed. * $P < 0.05$, ** $P < 0.01$, *** $P < 0.001$, **** $P < 0.0001$.

revealed that there was no significant interaction among sex, hM3Dq expression, and CNO treatment on duration investigating both a lego ($F(1, 82) = 0.1443, P > 0.70$) or a novel mouse ($F(1, 81) = 1.899, P > 0.17$). Subsequent post hoc analyses indicated that male *Crh:hM3Dq* mice treated with CNO spent significantly less time ($P < 0.01$) interacting with female mice (Fig. 4J and *SI Appendix, Fig. S10A*) with no difference in social preference index (*SI Appendix, Fig. S11B*). We detected no significant changes in social behaviors in female *Crh:hM3Dq* mice treated with CNO (Fig. 4J and *SI Appendix, Fig. S11B*). We also observed that female mice injected with the hM3Dq virus prefer the lego compared to males injected with the hM3Dq virus both with or without CNO, and that control males prefer a novel mouse compared to control females independently of CNO (Fig. 4J). These analyses also show that in the absence of CNO, male injected with the hM3Dq virus shows a significant preference for a novel mouse compared to female injected with the hM3Dq virus (Fig. 4J). In the novel object recognition test (Fig. 4K), three-way ANOVA revealed that there was no significant interaction among sex, hM3Dq expression, and CNO treatment on duration investigating for both a familiar ($F(1, 94) = 0.7971, p > 0.37$) and novel mouse ($F(1, 92) = 1.055, p > 0.30$). Post hoc analyses were again conducted and we observed that chemogenetic activation of mPFC *Crh:hM3Dq* in male mice, not in female mice, significantly reduced the exploration time of a novel object over a familiar object ($P < 0.05$, Fig. 4K and *SI Appendix, Fig. S10B*). These behaviors indicate that activation of mPFC *Crh:hM3Dq* via CNO decreases novelty exploration selectively in males while not affecting anxiety-like behaviors. In the novel object recognition test, we observed that CNO-affected female mice injected with the control virus AAV-mCherry, although the differences were not significant ($P > 0.39$; Fig. 4K). We also observed that CNO-affected control females in the elevated plus maze and in the open field test (*SI Appendix, Fig. S9*). It is possible that metabolites of CNO such as clozapine, shown to produce clozapine-like interoceptive stimulus effects in rats and mice may cause off-target effects in females (45). Taken together, our data establish that the behavioral states regulated by local *Crh* in the mPFC of males are distinct from those governed by its release from afferent fibers originating in the hypothalamus, and they contribute to the modulation of male-specific novelty exploration.

Discussion

Information processing in the cerebral cortex is dependent on a wide variety of interneuron types that gate signal flow and modulate local circuitry (46, 47). Cortical interneurons often express specific neuropeptides, hormones, and other neuromodulatory substances in addition to fast-acting neurotransmitters (13). In those cases where neuromodulators are expressed both in distal sites that project to the cerebral cortex and in local interneurons, it is not known whether the source of production contributes differentially to function. Here we have focused on CrhINs in the mPFC to determine whether neurotransmitters and neuromodulators produced in a single interneuron class function synergistically, to delineate how CrhINs modulate local circuit function in the mPFC and to explore the distinct role of locally produced CRH in complex, sex-specific behaviors.

The data we have reported demonstrate that CrhINs release GABA which acts directly to inhibit OxtRINs (a subset of SST interneurons) and L2/3 PCs. CrhINs also release CRH upon high-frequency stimulation selectively in male mice and released CRH increases the excitability of nearby L2/3 PCs expressing the CRHR1 receptor to modulate male-specific novelty exploration. The ability of CrhINs

to directly inhibit OxtRINs is interesting given previous data demonstrating that they release CRHBP, which can bind to and inhibit the actions of CRH (16). Under conditions of high-frequency stimulation of CrhINs that is required for the release of CRH and excitation of CRHR1 expressing L2/3 pyramidal cells, this blockade of CRHBP release can act synergistically with local CRH to maximize its impact in the mPFC. Given our previous studies of the roles of OxtRINs in female sociosexual behavior (15) and male anxiety-related behaviors (16), these data identify these two sparse interneuron populations as reciprocal partners regulating local mPFC circuits involved in the modulation of complex, sex-specific behaviors. Although the precise circuit architecture and molecular mechanisms delineated in these studies have not been previously reported, they are consistent with the complementary and often opposing biological functions of OXT and CRH in a wide variety of biological responses (48–50).

CRH neurons in the hypothalamus project to several brain structures (51, 52), including the cerebral cortex (Fig. 1). Deletion or loss of CRH production from hypothalamic neurons leads to a strong anxiolytic phenotype, as demonstrated by alterations of several approach avoidance behaviors in male mice (21). The finding that local production of CRH in the mPFC modulates different behaviors than those mediated by hypothalamic CRH release into the cortex (21) indicates that CRH release in the mPFC must impact local circuitry differently depending on its source of production. Although we have not directly addressed the mechanisms responsible for this difference, it seems likely that this reflects the observation that axons reaching the mPFC from CRH cells in the PVN appear to terminate in deeper cortical layers while CrhIN processes extend to the pial surface (Fig. 1H).

We report that CRH release from mPFC interneurons requires high-frequency stimulation that induces CRH release selectively in male mice (Fig. 3). This difference between male and female mice cannot be explained by either reduced CRHR1 levels or increased *Crhbp* expression in female mice as both TRAP and RT-PCR found that male and female mice express comparable levels of *Crhr1* and *Crhbp* in the mPFC (16). Future studies will be needed to investigate the mechanisms underlying the male-specific CRH release from CrhINs in the mPFC upon high-frequency stimulation. Since deletion of *Crh* from CrhINs neurons alters male-specific novelty-seeking behaviors (Fig. 4) and these neurons are capable of firing repetitive APs in response to small hyperpolarizing current injections (Fig. 1 J–L and *SI Appendix, Fig. S5A*), identification of afferents that might stimulate burst firing of CrhINs in vivo is a further step toward understanding this circuit. A candidate for this role is suggested by the finding that CrhINs express 5-HT_{3A}R (Fig. 1B), the only ionotropic serotonin receptor. Since activation of this receptor by serotonin (5-HT) causes fast depolarizing currents (53), since its specific agonist, mCPBG elicits high-frequency firing of 5-HT_{3A}R expressing interneurons (20), and since 5-HT_{3A}R expressing interneurons in the cerebral cortex receive direct monosynaptic input from dorsal raphe serotonergic neurons (54), it seems likely that release of 5-HT from the dorsal raphe nucleus could act on this small subset of CrhIN/5-HT_{3A}R expressing interneurons to cause burst firing and CRH release thereby inhibiting male novelty exploration. The release of CRH from the hypothalamic PVN into the cortex is not likely to be modulated by this mechanism because little to no expression of 5-HT_{3A}R is evident in the PVN. Further studies will be required to determine whether stimulation of CrhINs by dorsal raphe axons in the mPFC results in CRH release, and to understand the conditions that activate this pathway to modulate male novelty exploration.

In rodents, the mPFC can be divided into different subregions: the anterior cingulate cortex (ACC), the prelimbic cortex (PL), and the infralimbic cortex (IL) although there is no clear consensus

(55). The ACC, PL, and IL have been shown to play different roles (56–58). It has been hypothesized that the PL is essential for developing goal-directed response strategies, while the IL supports habit behavior. Also, it has been proposed that some functions of the orbital PFC parallel those of the mPFC in the regulation of response selection (58). In this study, we conducted stereotaxic viral injections into the PL region of the mPFC for electrophysiological and behavioral studies. Therefore, we can conclude that CrhINs in the PL region of the mPFC modulate male-specific novelty exploration. Future studies will be needed to investigate whether the other subregions in the mPFC, ACC, and IL would also alter novelty exploration in a sex-specific manner. While the questions of whether rodent and primate mPFC share similar functional organization, and whether they are functionally analogous to the primate lateral prefrontal cortex are controversial (59), the molecular mechanisms we have identified here may be relevant for development of strategies for normalization of novelty exploration in boys and men. Given the facts that patients in autism spectrum disorder (ASD) have been reported to be less responsive to novel stimuli (60, 61), and that more males are diagnosed with ASD than females (62–64), agents that inhibit CrhINs activity in the cortex may help correct the reduced interest in novelty evident in some male patients with ASD.

Materials and Methods

Mice. All animal procedures were approved by The Rockefeller University Institutional Animal Care and Use Committee and were in accordance with NIH guidelines. CRH-IRES-Cre, Crh:FLOX, and VIP-IRES-Flp mice were purchased from Jackson Laboratory (012704, 030110, 016962, 028578). Oxt-Cre mice were generated by The Rockefeller University GENSAT Project. CRH-IRES-Flp mice were generously donated by the laboratory of Dr. Bernardo Sabatini. Mice were group housed, up to 5 per cage. Mice were always allowed ad libitum access to food and water, weaned at 3 wk of age, and maintained on 12-h light/dark cycle.

TRAP-seq. The TRAP procedure was performed as described previously (Mellén et al., 2012) and described in detail in *SI Appendix*.

Viral Stereotaxic Surgeries. Stereotaxic surgeries were performed on 7–8-wk-old mice. Anesthetized mice were located in a stereotaxic adaptor (Stoelting Co), and bilateral injections ($4 \times 0.25 \mu\text{l}$) were performed targeting the mPFC (in mm: AP +1.90 and +1.65, ML ± 0.25 , DV -2.00). The AAV viruses and mouse strains used can be found in *SI Appendix*. Mice recovered for at least 4 wk prior to behavioral and electrophysiological studies.

Brain Slice Preparation and Electrophysiological Recordings. Fourteen-to-fifteen-week-old mice were anesthetized with ketamine and perfused with dissection buffer. Brains were sectioned, allowed to recover in artificial cerebrospinal fluid (aCSF), and brain slices were transferred to the recording chamber constantly perfused in aCSF with 95% O₂/5% CO₂ gas, and temperature controlled to 32°C. Four to eight M Ω glass capillary pipettes were pulled and filled with internal solution for current clamp or voltage clamp. Recordings were made using a Scientifica SliceScope Pro 1000 with data filtered at 2.4 kHz and digitized at 10 kHz using a Digidata 1440A interface (Molecular Device) driven by pClamp 9.2 (Molecular Device). The composition of buffers and more details are given in *SI Appendix*.

Immunohistochemistry. Mice were deeply anesthetized and perfused. Brains were dissected, postfixed, and submerged in 30% sucrose prior to sectioning. Brains were frozen in dry ice and sectioned using a Leica SM2000R Sliding Microtome at 40 μm . Sections were stored in cryoprotectant solution at -20°C , rinsed thoroughly and incubated in the corresponding primary and secondary antibodies as described in *SI Appendix*. Brain slices were imaged on a Zeiss LSM700 confocal microscope, and stored at 4°C.

Fluorescence In Situ Hybridization (FISH). FISH was conducted using RNAscope Multiplex Fluorescent Reagent Kit v2 (Advanced Cell Diagnostics 323100). More details can be found in *SI Appendix*.

Behavioral Tests. Three-to-four-month-old mice underwent an array of behavioral paradigms with at least 5 d between different tests. The experimenter was blind to the treatment for each group except for the Crh:hM3Dq CNO and vehicle injections. Specific details on the elevated plus maze, open-field test, light/dark box, three-chamber sociability test and novel object recognition test can be found in *SI Appendix*. Following behavioral testing, mice were subject to immunohistochemistry to validate viral expression.

Statistical Analyses. Data are presented as means \pm SEM. Statistical analyses were performed with Two-way ANOVA, except when comparing two groups in one condition, where Student's *t* test was used. Statistical analyses were made using GraphPad Prism. We regarded the data as statistically significant when *P* values were lower than 0.05.

Data, Materials, and Software Availability. All study data are included in the article and/or *SI Appendix* and TRAP data have been deposited in NCBI's Gene Expression Omnibus (Edgar et al., 2002) and are accessible through GEO Series accession number GSE6549996, GSE6549997, GSE6549999, and GSE6550000, (<https://www.ncbi.nlm.nih.gov/geo/query/acc.cgi?acc=GSE6549996>).

ACKNOWLEDGMENTS. We thank all the members of the Heintz lab for helpful discussions and technical help. In particular, we thank Dr. Kun Li, Cuidong Wang, Sylvia M. Lipford, Dr. Elitsa Stoyanova, Nicholas Didkovsky, and Laura Kus. This research was supported by the HHMI and NIDA UG3-UH3 DA048385 (K.P. and I.I.-T.).

1. B. Tasic et al., Adult mouse cortical cell taxonomy revealed by single cell transcriptomics. *Nat. Neurosci.* **19**, 335–346 (2016).
2. J. P. Doyle et al., Application of a translational profiling approach for the comparative analysis of CNS cell types. *Cell* **135**, 749–762 (2008).
3. C. Luo et al., Single-cell methylomes identify neuronal subtypes and regulatory elements in mammalian cortex. *Science* **357**, 600–604 (2017).
4. X. Xu et al., Species and cell-type properties of classically defined human and rodent neurons and glia. *eLife* **7**, e37551 (2018).
5. S. R. y. Cajal, *Comparative Study of the Sensory Areas of the Human Cortex* (Clark University, 1899).
6. V. Kozareva et al., A transcriptomic atlas of mouse cerebellar cortex comprehensively defines cell types. *Nature* **598**, 214–219 (2021).
7. F. Scala et al., Phenotypic variation of transcriptomic cell types in mouse motor cortex. *Nature* **598**, 144–150 (2021).
8. N. W. Gouwens et al., Classification of electrophysiological and morphological neuron types in the mouse visual cortex. *Nat. Neurosci.* **22**, 1182–1195 (2019).
9. P. Ghaderi, H. R. Marateb, M. S. Safari, Electrophysiological profiling of neocortical neural subtypes: A semi-supervised method applied to in vivo whole-cell patch-clamp data. *Front. Neurosci.* **12**, 823 (2018).
10. A. Zeisel et al., Molecular architecture of the mouse nervous system. *Cell* **174**, 999–1014.e1022 (2018).
11. C. I. Bargmann, Beyond the connectome: How neuromodulators shape neural circuits. *Bioessays* **34**, 458–465 (2012).
12. E. Marder, D. Bucher, Understanding circuit dynamics using the stomatogastric nervous system of lobsters and crabs. *Annu. Rev. Physiol.* **69**, 291–316 (2007).
13. A. J. Granger, M. L. Wallace, B. L. Sabatini, Multi-transmitter neurons in the mammalian central nervous system. *Curr. opin. Neurobiol.* **45**, 85–91 (2017).
14. K. M. Smith et al., Calretinin positive neurons form an excitatory amplifier network in the spinal cord dorsal horn. *eLife* **8**, e49190 (2019).
15. M. Nakajima, A. Gorlich, N. Heintz, Oxytocin modulates female sociosexual behavior through a specific class of prefrontal cortical interneurons. *Cell* **159**, 295–305 (2014).
16. K. Li, M. Nakajima, I. Ibanez-Tallon, N. Heintz, A cortical circuit for sexually dimorphic oxytocin-dependent anxiety behaviors. *Cell* **167**, 60–72 (2016).
17. P. Chen et al., Prefrontal cortex corticotropin-releasing factor neurons control behavioral style selection under challenging situations. *Neuron* **106**, 301–315.e307 (2020).
18. Y. Peng, F. J. Barreda Tomas, C. Klisch, I. Vida, J. R. P. Geiger, Layer-specific organization of local excitatory and inhibitory synaptic connectivity in the rat presubiculum. *Cereb. Cortex* **27**, 2435–2452 (2017).
19. A. Uribe-Marino et al., Prefrontal cortex corticotropin-releasing factor receptor 1 conveys acute stress-induced executive dysfunction. *Biol. Psychiatry* **80**, 743–753 (2016).
20. S. Lee, J. Hjerling-Lefler, E. Zagha, G. Fishell, B. Rudy, The largest group of superficial neocortical GABAergic interneurons expresses ionotropic serotonin receptors. *J. Neurosci.* **30**, 16796–16808 (2010).
21. R. Zhang et al., Loss of hypothalamic corticotropin-releasing hormone markedly reduces anxiety behaviors in mice. *Mol. Psychiatry* **22**, 733–744 (2017).
22. H. Taniguchi et al., A resource of Cre driver lines for genetic targeting of GABAergic neurons in cerebral cortex. *Neuron* **71**, 995–1013 (2011).
23. T. Fuzesi, N. Daviu, J. I. Wamsteeker Cusulin, R. P. Bonin, J. S. Bains, Hypothalamic CRH neurons orchestrate complex behaviours after stress. *Nat. Commun.* **7**, 11937 (2016).
24. N. Dedic et al., Chronic CRH depletion from GABAergic, long-range projection neurons in the extended amygdala reduces dopamine release and increases anxiety. *Nat. Neurosci.* **21**, 803–807 (2018).

25. J. Peng *et al.*, A quantitative analysis of the distribution of CRH neurons in whole mouse brain. *Front. Neuroanat.* **11**, 63 (2017).
26. M. Heiman *et al.*, A translational profiling approach for the molecular characterization of CNS cell types. *Cell* **135**, 738–748 (2008).
27. C. K. Pfeffer, M. Xue, M. He, Z. J. Huang, M. Scanziani, Inhibition of inhibition in visual cortex: The logic of connections between molecularly distinct interneurons. *Nat. Neurosci.* **16**, 1068–1076 (2013).
28. D. J. Millman *et al.*, VIP interneurons in mouse primary visual cortex selectively enhance responses to weak but specific stimuli. *eLife* **9**, e5130 (2020).
29. J. G. Partridge *et al.*, Stress increases GABAergic neurotransmission in CRF neurons of the central amygdala and bed nucleus stria terminalis. *Neuropharmacology* **107**, 239–250 (2016).
30. L. Petreanu, D. Huber, A. Sobczyk, K. Svoboda, Channelrhodopsin-2-assisted circuit mapping of long-range callosal projections. *Nat. Neurosci.* **10**, 663–668 (2007).
31. L. Petreanu, T. Mao, S. M. Sternson, K. Svoboda, The subcellular organization of neocortical excitatory connections. *Nature* **457**, 1142–1145 (2009).
32. R. A. Pinol, R. Bateman, D. Mendelowitz, Optogenetic approaches to characterize the long-range synaptic pathways from the hypothalamus to brain stem autonomic nuclei. *J. Neurosci. Methods* **210**, 238–246 (2012).
33. J. Ren *et al.*, Habenula “cholinergic” neurons co-release glutamate and acetylcholine and activate postsynaptic neurons via distinct transmission modes. *Neuron* **69**, 445–452 (2011).
34. N. Toni *et al.*, Neurons born in the adult dentate gyrus form functional synapses with target cells. *Nat. Neurosci.* **11**, 901–907 (2008).
35. J. Wang, M. T. Hasan, H. S. Seung, Laser-evoked synaptic transmission in cultured hippocampal neurons expressing channelrhodopsin-2 delivered by adeno-associated virus. *J. Neurosci. Methods* **183**, 165–175 (2009).
36. Q. Xiong, H. V. Oviedo, L. C. Trotman, A. M. Zador, PTEN regulation of local and long-range connections in mouse auditory cortex. *J. Neurosci.* **32**, 1643–1652 (2012).
37. J. Szabadics *et al.*, Excitatory effect of GABAergic axo-axonic cells in cortical microcircuits. *Science* **311**, 233–235 (2006).
38. E. Arrigoni, C. B. Saper, What optogenetic stimulation is telling us (and failing to tell us) about fast neurotransmitters and neuromodulators in brain circuits for wake-sleep regulation. *Curr. Opin. Neurobiol.* **29**, 165–171 (2014).
39. M. Muschol, B. M. Salzberg, Dependence of transient and residual calcium dynamics on action-potential patterning during neuropeptide secretion. *J. Neurosci.* **20**, 6773–6780 (2000).
40. C. Schone, J. Apergis-Schoute, T. Sakurai, A. Adamantidis, D. Burdakov, Coreleased orexin and glutamate evoke nonredundant spike outputs and computations in histamine neurons. *Cell Rep.* **7**, 697–704 (2014).
41. T. Haug, J. F. Storm, Protein kinase A mediates the modulation of the slow Ca(2+)-dependent K(+) current, I(sAHP), by the neuropeptides CRF, VIP, and CGRP in hippocampal pyramidal neurons. *J. Neurophysiol.* **83**, 2071–2079 (2000).
42. S. Kratzer *et al.*, Activation of CRH receptor type 1 expressed on glutamatergic neurons increases excitability of CA1 pyramidal neurons by the modulation of voltage-gated ion channels. *Front. Cell Neurosci.* **7**, 91 (2013).
43. C. Inda *et al.*, Different cAMP sources are critically involved in G protein-coupled receptor CRHR1 signaling. *J. Cell Biol.* **214**, 181–195 (2016).
44. N. Dedic *et al.*, Deletion of CRH From GABAergic forebrain neurons promotes stress resilience and dampens stress-induced changes in neuronal activity. *Front. Neurosci.* **13**, 986 (2019).
45. D. F. Manvich *et al.*, The DREADD agonist clozapine N-oxide (CNO) is reverse-metabolized to clozapine and produces clozapine-like interoceptive stimulus effects in rats and mice. *Sci. Rep.* **8**, 3840 (2018).
46. H. Barbas, General cortical and special prefrontal connections: Principles from structure to function. *Annu. Rev. Neurosci.* **38**, 269–289 (2015).
47. R. Tremblay, S. Lee, B. Rudy, GABAergic interneurons in the neocortex: From cellular properties to circuits. *Neuron* **91**, 260–292 (2016).
48. D. K. Grammatopoulos, E. W. Hillhouse, Activation of protein kinase C by oxytocin inhibits the biological activity of the human myometrial corticotropin-releasing hormone receptor at term. *Endocrinology* **140**, 585–594 (1999).
49. M. Bulbul *et al.*, Hypothalamic oxytocin attenuates CRF expression via GABA(A) receptors in rats. *Brain Res.* **1387**, 39–45 (2011).
50. I. D. Neumann, A. Wigger, L. Torner, F. Holsboer, R. Landgraf, Brain oxytocin inhibits basal and stress-induced activity of the hypothalamo-pituitary-adrenal axis in male and female rats: Partial action within the paraventricular nucleus. *J. Neuroendocrinol.* **12**, 235–243 (2000).
51. G. Aguilera, Y. Liu, The molecular physiology of CRH neurons. *Front. Neuroendocrinol.* **33**, 67–84 (2012).
52. D. M. Vazquez *et al.*, Brain corticotropin-releasing hormone (CRH) circuits in the developing rat: Effect of maternal deprivation. *Brain Res.* **1121**, 83–94 (2006).
53. V. Derkach, A. Surprenant, R. A. North, 5-HT₃ receptors are membrane ion channels. *Nature* **339**, 706–709 (1989).
54. S. Zhang *et al.*, Whole-brain mapping of monosynaptic afferent inputs to cortical CRH neurons. *Front. Neurosci.* **13**, 565 (2019).
55. M. Laubach, L. M. Amarante, K. Swanson, S. R. White, If anything what, Is rodent prefrontal cortex? *eNeuro* **5**, ENEURO.0315-18.2018 (2018).
56. T. F. Giustino, S. Maren, The role of the medial prefrontal cortex in the conditioning and extinction of fear. *Front. Behav. Neurosci.* **9**, 298 (2015).
57. G. Q. Wang *et al.*, Deactivation of excitatory neurons in the prelimbic cortex via Cdk5 promotes pain sensation and anxiety. *Nat. Commun.* **6**, 7660 (2015).
58. S. L. Gourley, J. R. Taylor, Going and stopping: Dichotomies in behavioral control by the prefrontal cortex. *Nat. Neurosci.* **19**, 656–664 (2016).
59. D. J. Schaeffer *et al.*, Divergence of rodent and primate medial frontal cortex functional connectivity. *Proc. Natl. Acad. Sci. U.S.A.* **117**, 21681–21689 (2020).
60. G. Dawson *et al.*, Neural correlates of face and object recognition in young children with autism spectrum disorder, developmental delay, and typical development. *Child Dev.* **73**, 700–717 (2002).
61. H. van Engeland, J. W. Roelofs, M. N. Verbaten, J. L. Slagen, Abnormal electrodermal reactivity to novel visual stimuli in autistic children. *Psychiatry Res.* **38**, 27–38 (1991).
62. A. K. Halladay *et al.*, Sex and gender differences in autism spectrum disorder: Summarizing evidence gaps and identifying emerging areas of priority. *Mol. Autism* **6**, 36 (2015).
63. M. Kirkovski, P. G. Enticott, P. B. Fitzgerald, A review of the role of female gender in autism spectrum disorders. *J. Autism Dev. Disorders* **43**, 2584–2603 (2013).
64. M. C. Lai, M. V. Lombardo, S. Baron-Cohen, Autism. *Lancet* **383**, 896–910 (2014).